ELSEVIER

Journal of Structural Geology 27 (2005) 1563–1576

JOURNAL OF STRUCTURAL GEOLOGY

www.elsevier.com/locate/jsg

Neocrystallization, fabrics and age of clay minerals from an exposure of the Moab Fault, Utah

John G. Solum*, Ben A. van der Pluijm, Donald R. Peacor

Department of Geological Sciences, University of Michigan, 425 E. University Ave., 2534 C. C. Little Bldg. Ann Arbor, MI 48109-1063, USA

Received 25 January 2005; received in revised form 5 April 2005; accepted 8 May 2005
Available online 21 July 2005

Abstract

Pronounced changes in clay mineral assemblages are preserved along the Moab Fault (Utah). Gouge is enriched up to ~40% in $1M_d$ illite relative to protolith, whereas altered protolith in the damage zone is enriched ~40% in illite–smectite relative to gouge and up to ~50% relative to protolith. These mineralogical changes indicate that clay gouge is formed not solely through mechanical incorporation of protolith, but also through fault-related authigenesis. The timing of mineralization is determined using $^{40}Ar/^{39}Ar$ dating of size fractions of fault rocks with varying detrital and authigenic clay content. We applied Ar dating of illite–smectite samples, as well as a newer approach that uses illite polytypes. Our analysis yields overlapping, early Paleocene ages for neoformed ($1M_d$) gouge illite (63 ± 2 Ma) and illite–smectite in the damage zone (60 ± 2 Ma), which are compatible with results elsewhere. These ages represent the latest period of major fault motion, and demonstrate that the fault fabrics are not the result of recent alteration.

The clay fabrics in fault rocks are poorly developed, indicating that fluids were not confined to the fault zone by preferentially oriented clays; rather we propose that fluids in the illite-rich gouge were isolated by adjacent lower permeability, illite–smectite-bearing rocks in the damage zone.

Keywords: Clay gouge; $^{40}Ar/^{39}Ar$ dating; Moab Fault

1. Introduction

Clay gouge in faulted sedimentary rocks, a factor in predicting the sealing behavior of faults, is often described in terms of shale smear, or shale gouge ratio (e.g. Yielding et al., 1997; Jones and Hillis, 2003). This reflects a school of thought that clay gouge forms dominantly through the mechanical incorporation of protolith clays into a fault zone. While this is true in some settings, it does not entirely account for clay gouge formation, as fault-related clay mineralization can also be significant (Vrolijk and van der Pluijm, 1999; Yan et al., 2001). Several studies have described the gouge along the Moab Fault from a mechanical point of view (Foxford et al., 1998; Garden et al., 2001; Davatzes and Aydin, 2005). We explore the nature of fault-related clay mineralization in a well-exposed outcrop of the Moab Fault. We track fault-related changes in clay mineralogy by quantifying concentrations of both illite polytypes ($2M_1$ and $1M_d$) and discrete illite/mixed-layer illite–smectite (I–S). This combination of techniques improves upon earlier methods that used only discrete illite/mixed-layer I–S, and allows clay gouge to be directly dated, as discussed below.

Studies of clays in fault zones also have implications for fault mechanics. Observations of many natural faults indicate that they are mechanically weaker than predicted from Byerlee's Law (Kanamori and Anderson, 1975; Lachenbruch and Sass, 1980; Mount and Suppe, 1987; Zoback, 2000). Elevated fluid pressure and a corresponding reduction in effective stress is a favored cause of weak-fault behavior (Hubbert and Rubey, 1959; Sibson, 1990, 2003; Rice, 1992; Faulkner and Rutter, 2001). Clay growth in fault zones and the influence of clays on the permeability structure of fault zones have also been suggested as explanations for such weak-fault behavior (Wang, 1984; Rice, 1992). This scenario requires a mechanism that

* Corresponding author. Present address: Earthquake Hazards Team, US Geological Survey, 345 Middlefield Road, MS977, Menlo Park, CA 94025-3591, USA. Tel.: +1 650 329 4857; fax: +1 650 329 5143.
E-mail address: jsolum@usgs.gov (J.G. Solum).

0191-8141/$ - see front matter © 2005 Elsevier Ltd. All rights reserved.
doi:10.1016/j.jsg.2005.05.002

confines fluids to the fault core and prevents them from escaping through zones of otherwise fractured host rock. A well-developed clay fabric developed parallel to the fault has been suggested as one mechanism (e.g. Faulkner and Rutter, 2001). However, few quantitative measurements have been made of clay fabrics in fault zones, although the development of fault-parallel zones of fine-grained material have been observed in natural (e.g. Evans et al., 1997) and artificial gouge (Scruggs and Tullis, 1998; Zhang et al., 1999; Zhang and Cox, 2000). This study helps to address that problem.

2. Geologic setting

The Moab Fault (Fig. 1), located in east central Utah, is a normal fault with a long and complex history of deformation and fluid flow. The movement and dissolution of salt from the Paradox Formation has dominated the geologic history of this region of the Colorado Plateau from the time of salt deposition in the Pennsylvanian until the present (Huntoon, 1988; Oviatt, 1988). Moab Fault growth began in the Triassic in response to salt tectonism (Doelling, 1988). Subsequently, the Moab Fault grew intermittently throughout the Mesozoic and into the Tertiary (Foxford et al., 1996, 1998). While Tertiary reactivation is likely salt-related, several alternate causes for this reactivation have been proposed (Olig et al., 1996).

The history of fluid flow in and around the Moab Fault has been documented through examinations of stable isotopes (Pevear et al., 1997), manganese mineralization (Chan et al., 2001), calcite cementation, and reduction fronts (Garden et al., 2001). These studies demonstrate that fluid flow in and around the Moab Fault zone has occurred.

Olig et al. (1996) divided the Moab Fault into a northern (16 km long), a central (19 km long), and a southern section (19 km long). The study site for this paper is located along the central section, which accommodated the most displacement (Olig et al., 1996). A single well-preserved exposure of the Moab Fault was characterized in great detail as part of this study (Fig. 2). The fault is composed of a main strand with a throw of ~900 m, and a minor strand with a throw of ~60 m (Foxford et al., 1998). The Pennsylvanian Honaker Trail Formation and Permian Cutler Group and the Jurassic Entrada Formation are juxtaposed across the main strand, and the Entrada Formation is juxtaposed against the Salt Wash Member of the Jurassic Morrison Formation across the minor fault. The stratigraphy of the study area is shown in Table 1. The main fault strand consists of a gouge zone, or fault core (using the terminology of Caine et al. (1996)), that is 1–2 m wide. The gouge zone has a mesoscopic fabric that is often fault parallel, but with a variable attitude that includes several zones where the fabric is at a high angle to the fault. The gouge is clay-rich with occasional clasts of comminuted quartz sandstone derived from the country rock, and is bound by a region of less intensely deformed material (the damage zone using the classification of Caine et al., 1996). This zone is characterized by fractured and cataclastically deformed sandstones and shales from the Permian Cutler group, although discontinuous bedding is still visible and in some instances it can be traced to undeformed bedding farther from the fault. For the purposes of this study, the minor fault and the trapped sliver of the Entrada Formation are included as part of the damage zone of the major fault strand. The damage zone is bound by undisturbed protolith at both sides of the fault zone.

The study described in this paper will examine the involvement of clays in a well-exposed extensional fault zone. The objectives of this study are to (1) quantify fault-related clay neomineralization; (2) quantify fabrics in clay-rich fault rocks and protolith; (3) use the above characterizations to date the fault fabric using a modified version of the illite dating technique described in van der Pluijm et al. (2001); and (4) hypothesize how fault-related clay neomineralization and fabric development may influence the permeability structure of the fault zone.

3. Methods

3.1. Illite and illite–smectite

3.1.1. Sampling

Seventeen samples were collected from a traverse across the Moab Fault zone, including eight samples from the Salt Wash Member of the Morrison Formation (collected from a shale-rich bed at distances of 2–59 m from the fault core), two samples of the Cutler Formation (collected from 8 to 9 m from the fault core), three samples of clay gouge (two from the main strand, one from the minor strand), and four samples from the damage zone derived from the Cutler Formation (at distances from 0 to 8 m from the fault core). The outer 10–20 cm of material was removed from sampling locations to allow the collection of samples that were uncontaminated by surface weathering. In order to eliminate interference on diffractograms from non-clay minerals, the <4 μm size fraction was extracted from all samples. Samples were prepared in a jaw crusher, suspended in water, and ultrasonically disaggregated. Following this, the suspensions were allowed to settle and the <4 μm size fractions were extracted.

3.1.2. Illite polytypism

Illite occurs as two polytypes, $2M_1$ and $1M_d$, which reflects variations in the way clay mineral interlayering is uniquely arranged for individual polytypes. In the $2M_1$ polytype, the stacking is ordered, alternate layers being related by rotations of 180° about the layer normal, resulting in stacking with a periodicity of 2 nm (20 Å). In the ideal $1M_d$ polytype, all layers are related by different rotation angles. These rotational variations can be detected through either X-ray diffraction

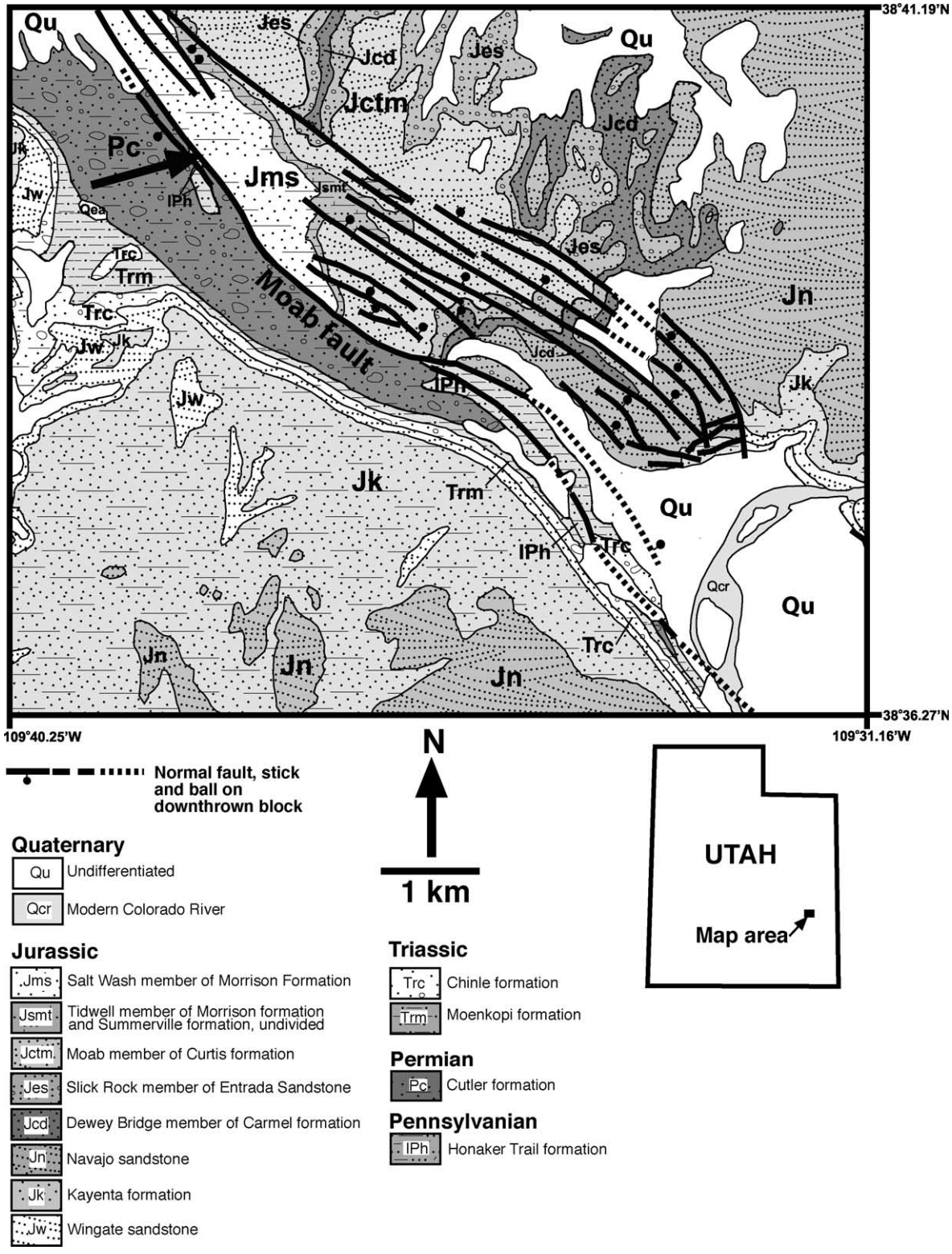

Fig. 1. Geologic map of the Moab, Utah, area (after Doelling, 2001). The study site is denoted by a black arrow, and is the R191 Canyon outcrop of Foxford et al. (1998).

(XRD) or selected area electron diffraction (SAED) using transmission electron microscopy (TEM).

Using XRD, it is possible to quantify the relative amounts of $2M_1$ and $1M_d$ illite, as well as the proportion of discrete illite to I–S, as discussed below. The amount of $2M_1$ illite may be quantified using XRD patterns from a randomly oriented sample, achieved using a side packing device as described by Moore and Reynolds (1997). It is

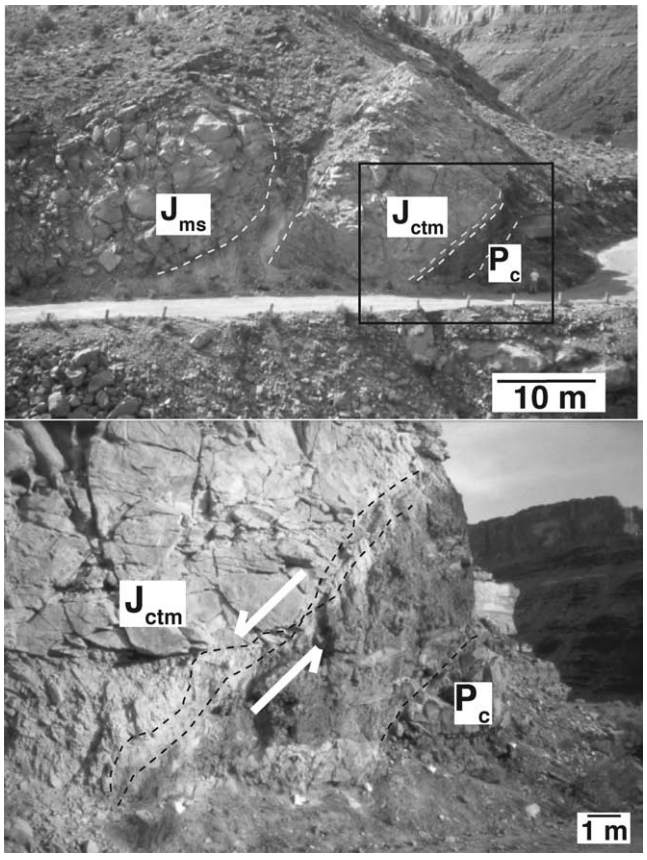

Fig. 2. Outcrop photographs of the study area. At this location, Pennsylvanian and Permian shales and sandstones (Honaker Trail Formation and Cutler Group) are juxtaposed against Jurassic formations (sandstones and shales of the Entrada and Morrison Formations) and are separated by a gouge zone ~1–2 m wide. The fault has a throw of ~960 m at this location. A minor strand of the fault with a throw of ~60 m is shown as a dashed line.

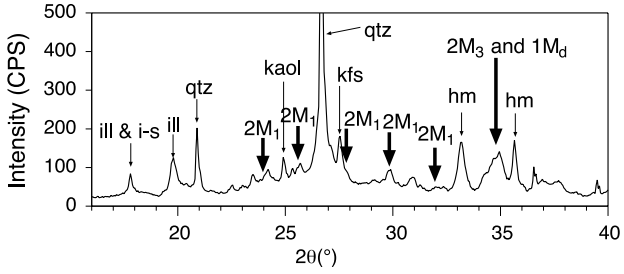

Fig. 3. The amount of $2M_1$ illite is quantified using X-ray diffraction patterns from randomly oriented samples, which enhances the intensity of the diagnostic non-(00*l*) $2M_1$ illite peaks. The area of peaks that are unique to the $2M_1$ polytype (labeled '$2M_1$') divided by the area of a peak at ~35° 2θ that is common to both polytypes (labeled '$2M_1$ and $1M_d$') is a function of the concentration of $2M_1$ and $1M_d$ illite, which can be quantified using the method of Grathoff and Moore (1996). All five $2M_1$-specific peaks cannot necessarily be used on each sample due to overlap with other minerals, such as K-feldspar. Unused illite and I–S peaks or peaks belonging to other phases are abbreviated as follows: illite (ill), I–S (i–s), quartz (qtz), kaolinite (kaol) K-feldspar (kfs) and hematite (hm).

critical to obtain a sample with a random orientation because the peaks that are diagnostic of polytypes have non-(001) indices that are absent in oriented samples. The concentration of the $2M_1$ polytype is determined by measuring the area of five peaks that are unique to the $2M_1$ polytype and ratioing them against the area of a peak at ~0.258 nm (2.58 Å)/35° 2θ (Cu Kα), which is common to both polytypes (Grathoff and Moore, 1996) (Fig. 3). The technique of Grathoff and Moore (1996) represents a significant improvement over earlier techniques, which relied on the measurement of only one $2M_1$-specific peak, such as from Hower et al. (1963), summarized in Grathoff and Moore (1996). In this study, the randomness of samples was evaluated by comparing the relative intensity of the (100) quartz peak at 0.4257 nm (4.257 Å)/20.8° 2θ (Cu Kα) and the (004) illite peak at 0.502 nm (5.02 Å)/17.65° 2θ (Cu Kα) on both side-packed and oriented sample preparations. We do not report the concentration of 1M illite (cf. Grathoff and Moore, 1996; Grathoff et al., 1998), because TEM investigations of shales, mudstones and slates, inferred to contain 1M illite using XRD, have almost exclusively been unable to find the proposed illite polytype (Peacor et al., 2002). This is also in agreement with the suggestion of Zoller and Brockamp (1997), who concluded that $2M_1$ and 1M illite differ in composition and therefore are not polytypes sensu stricto. In this study, the amount of $2M_1$ illite was therefore determined, assuming that the remaining illite is the $1M_d$ polytype, which was validated by our TEM studies that detected only the $2M_1$ and $1M_d$ polytypes of illite. Differences in polytypism, relatively subtle on X-ray powder diffraction patterns, are readily apparent on SAED patterns (Fig. 4). Verification that a given grain is illite was made using the spacing of the (001) reflection, which is 1 nm (10 Å). The $2M_1$ and $1M_d$ polytypes are distinguished using (hk0) reflections, which occur as discrete spots in $2M_1$ illite with a spacing of 20 Å, indicating that the stacking is ordered with a 20 Å periodicity. These reflections are streaked, non-periodic and diffuse in $1M_d$ illite, indicating that the stacking sequence is disordered. It is not possible to quantify the amounts of $2M_1$ and $1M_d$ illite using transmission electron microscopy due to the limited sample volume as well as difficulties finding illite grains with a favorable orientation such that the (hk0) reflections are visible on the SAED patterns.

3.1.3. Discrete illite and mixed-layer I–S

Grains containing both illite and smectite are known as I–S, and are classified by the number and degree of ordering of smectite- and illite-like interlayers. The number of interlayers is given by the percent smectite in a sample, and the ordering is expressed by 'Reichweite' (R), where R0 corresponds to random interlayering, R1 corresponds to alternating illite and smectite interlayers, R2 corresponds to two smectite interlayers followed by an illite, etc. The amount of I–S is determined using the program NEWMOD (Reynolds and Reynolds, 1996) by calculating powder

Table 1
Simplified stratigraphy of the Moab area (after Doelling et al., 1988, Table 1)

Age	Formation	Lithology	Thickness
Cretaceous	Mancos (upper, Ferron, and lower members)	Marine shale with some sandstone and sandy shale in the Ferron member	1080–1180 m
	Daktoa	Sandstone to conglomerate with some sandy shale	0–37 m
	Cedar Mountain	Silty mudstone with interbedded sandstone and conglomerate	12–76 m
Jurassic	Morrison (Brushy Basin, Salt Wash, and Tidwell members)	Brushy Basin member is mudstone with some sandstone, conglomerate and limestone. Salt Wash member is sandstone with interbedded mud- and siltstones. Tidwell member is silty shale	136–245 m
	Curtis. Moab member	Formerly Moab Tongue of the Entrada formation	0–42 m
	Entrada, Slick Rock member	Fine to medium eolian sandstone	43–152 m
	Carmel, Dewey Bridge member	Silty sandstone. Formerly Dewey Bridge member of the Entrada formation	8–72 m
	Navajo	Fine eolian sandstone	0–225 m
	Kayenta	Sandstone	30–90 m
	Wingate	Fine quartz sandstone	75–137 m
Triassic	Chinle	Silty sandstone and mudstone and gritstone	0–275 m
	Moenkopi	Sandy shale with micaceous silty sandstone	0–400 m
Permian	Cutler	Sandstone and conglomerate with micaceous sandy shales	0–2450 m
Pennsylvanian	Honaker Trail	Limestone, shale and sandstone	0–1525 m
	Paradox Formation	Evaporites with black shale and thin limestone and sandstone	0–1370 m

patterns for various mixtures of illite and I–S (with varying numbers and orderings of smectite interlayers) and visually comparing these synthetic powder patterns to the experimental powder patterns until a match is found (Fig. 5). In this case, sample preparations imparting a well-developed preferred orientation were used to enhance the intensities of the (001) peaks, which provide the most information about I–S. Oriented preparations were made by drying clay/water slurries on glass slides. The slides were placed in a chamber containing ethylene glycol to cause expansion of smectite interlayers, allowing for greater ease of detection of smectite-bearing phases on powder diffraction patterns.

3.2. Clay fabrics

Quantification of clay fabrics is complicated by very fine grain sizes. The fabric intensities of fault rock and protolith were measured using X-ray texture goniometry (XTG), which provides a reliable measure of the degree of alignment of clays (van der Pluijm et al., 1994). Twenty-four pole figures from seven hand samples from the gouge zone, damage zone and protolith were collected. With XTG, a ~200–400-μm-thick resin-impregnated sample is placed in a modified single-crystal X-ray diffractometer with a molybdenum source ($\lambda K\alpha = 0.707$ Å). The phases present in the sample are identified through collection of a diffractogram, and the detector is then moved to the value of 2θ, which corresponds to the (001) plane of the mineral to be analyzed ($d = 1$ nm (10 Å) for illite, 1–1.5 nm (10–15 Å) for I–S, 0.7 nm (7 Å) for kaolinite), and the sample is then automatically rotated through 1296 positions. The location and the intensity of the diffracted X-ray beam at each of those locations are plotted in an equal area projection and then contoured using multiples of a random distribution (MRD), a statistical measure of the randomness of a distribution that is functionally equivalent to percentage per 1% area (Wenk, 1985). The greater the MRD value, the 'higher' the peak on the equal area net, and the better aligned the clay fabric. In addition, scanning electron microscopy (SEM) was obtained from five thin sections and TEM images were obtained from four specimens to confirm the distributions of clay minerals in the samples. Anisotropy of magnetic susceptibility (AMS) has also been used to characterize clay fabrics (Hayman et al., 2004; Solum, 2005).

3.3. Gouge dating

As in other dating studies of fault rocks (e.g. Vrolijk and van der Pluijm, 1999; van der Pluijm et al., 2001), dating of Moab gouge is complicated by the presence of illite as a mixture of detrital and neoformed grains. The occurrence of multiple illite polytypes in clay-bearing samples, and variations between polytype composition and age, has long been recognized (Hower et al., 1963; Velde and Hower, 1963; Pevear, 1999). These workers found that in shales the age of the finest fraction (rich in I–S and disordered illite) was younger than the age of deposition, whereas the age of the coarsest fraction (rich in discrete $2M_1$ illite) was older. These observations indicate that the illite in the sample is composed of a detrital population and a neoformed authigenic population (e.g. Pevear, 1999).

As indicated above, any single gouge age is a mixing age, and has limited geological significance (Pevear, 1999). This

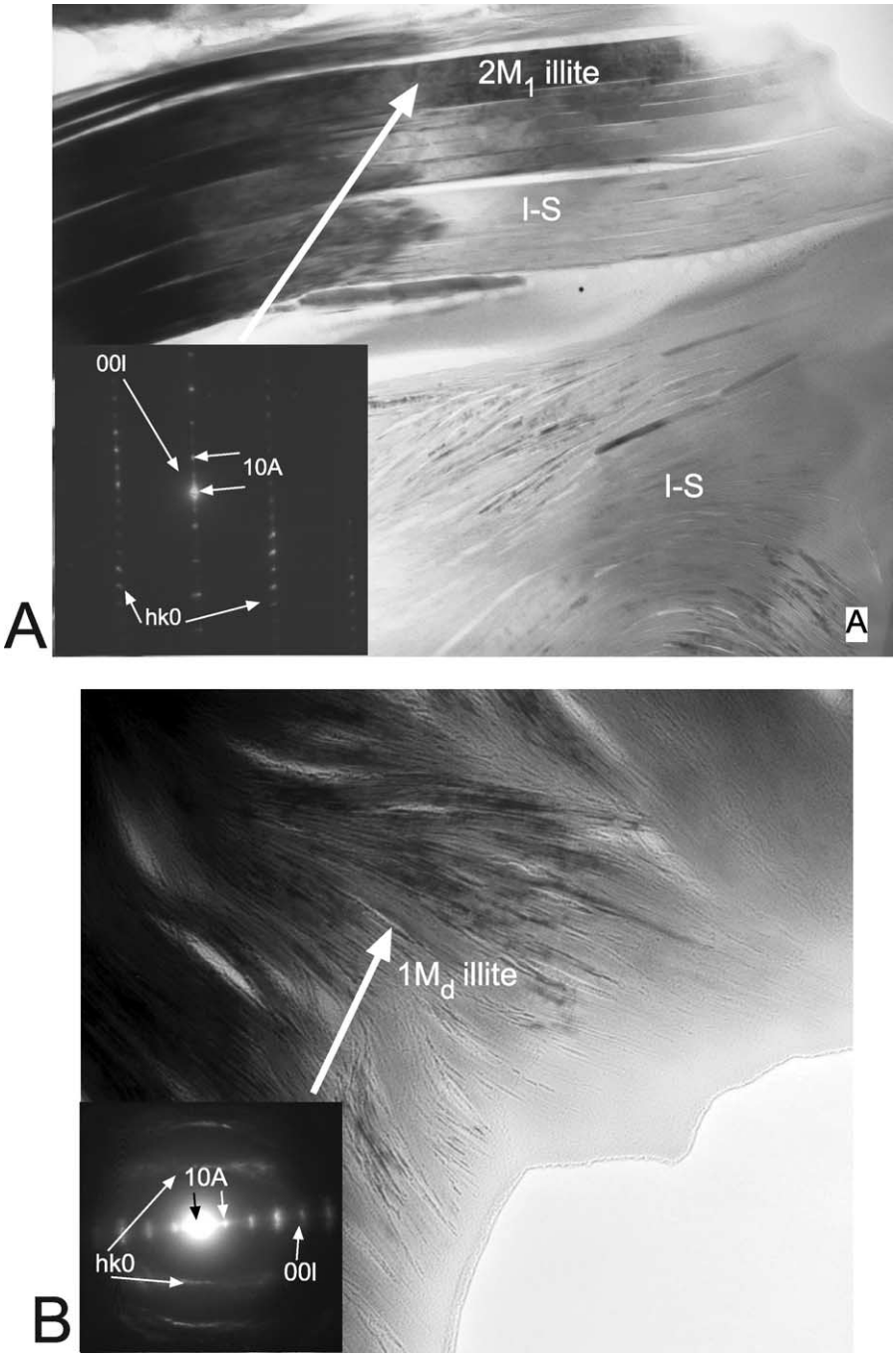

Fig. 4. Lattice fringe images and selected area electron diffraction patterns of $2M_1$ (A) and $1M_d$ illite (B). In both cases, the *d*-value of the (001) reflection is 1 nm (10 Å), indicating that the mineral is illite. The $2M_1$ and $1M_d$ polytypes are distinguished using the (hk0) spots. With $2M_1$ illite, these reflections occur as discrete spots. With $1M_d$ illite, the (hk0) reflections are streaked, indicating that stacking is disordered. The polytypes also have a characteristic appearance on lattice fringe images in that $1M_d$ illite is typically wavy. It is not possible to quantify the amounts of $2M_1$ and $1M_d$ illite using transmission electron microscopy due to an extremely limited sample volume as well as difficulties finding illite grains with a favorable orientation such that the (*hk*0) reflections are visible on the selected area electron diffraction patterns.

restriction is overcome by separating a sample into three size fractions; coarse (0.5–2 μm), medium (0.05–0.5 μm) and fine (<0.05 μm), and determining the proportion of detrital to authigenic illite for each of these fractions. There are two potential ways to quantify the amounts of detrital and authigenic material. The first is to use polytypism; the amount of $2M_1$ illite is equivalent to the amount of detrital illite, and the $1M_d$ polytype is equivalent to the neoformed fraction of the sample (see also Grathoff and Moore, 1996; Grathoff et al., 1998). The second is to quantify the amount of discrete illite and I–S. Discrete illite can be considered to be detrital and I–S to be authigenic (Pevear, 1999). In order

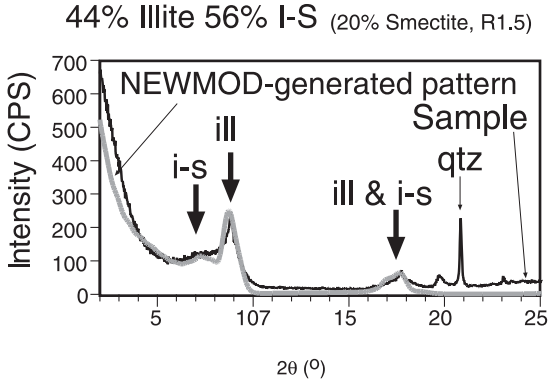

Fig. 5. The proportions of discrete illite and mixed-layer I–S are determined using the program NEWMOD to generate artificial powder patterns for various mixtures of illite and illite–smectite (with varying numbers of smectite interlayers). Quantification is achieved by visually comparing these synthetic powder patterns to the experimental powder patterns until a match is found. The parameters that can be varied are the amount of smectite interlayers and the ordering of the stacking of the smectite interlayers. Variations in illite and illite–smectite are expressed in (001) peaks, and only sample preparations in which there is a well-developed preferred orientation are used, so that the intensity of those peaks will be enhanced. Pz is the Paleozoic Cutler Formation, Mz is the Mesozoic.

to recognize detrital and authigenic clays, it is first necessary to identify the fault-related change(s) in the clay mineral assemblages: if $1M_d$ illite is neoformed (if fault rocks are enriched in $1M_d$ illite), then the proportion of $2M_1$ to $1M_d$ should be used; if I–S is formed (if fault rocks are enriched in I–S), then the proportion of discrete illite to I–S should be used. It should be noted that the two scenarios can be complementary. Once the proportion of detrital and neoformed illite is determined, each of the fractions is then dated using the $^{40}Ar/^{39}Ar$ technique after being encapsulated in a quartz vial to prevent argon loss due to recoil (for method see van der Pluijm et al. (2001)). The age spectra will not have plateaus due to argon recoil (Dong et al., 1995) and because they are composed of mixtures of grains of different ages. Therefore, the total gas age is used to determine the age of the sample. The age and the percent detrital illite of the coarse, medium, and fine fractions are plotted, and the extrapolated value that corresponds to 0% detrital ($2M_1$ and/or discrete illite) illite can be determined, corresponding to the age of the neoformed clays ($1M_d$ illite and/or I–S), and, therefore, to the age of the fault fabric (van der Pluijm et al., 2001; Ylagan et al., 2002). When applied to undeformed shales, the age corresponds to the timing of clay neomineralization during diagenesis (Pevear, 1999), or the age of clay neomineralization associated with a hydrothermal event (Grathoff et al., 2001).

The use of dating multiple gouge (or shale) size fractions coupled with clay characterizations has been previously applied (e.g. Hower et al., 1963; Lyons and Snellenburg, 1971; Parry et al., 2001; Zwingmann et al., 2004); however, these studies have not used the illite age analysis technique to extrapolate and age for uncontaminated/end-member neoformed clays. This study integrates both quantifications of discrete illite/mixed-layer I–S and $2M_1/1M_d$ polytypism to directly date fault rocks.

The use of detailed polytype quantification has been used to date fault zones only once before (Ylagan et al., 2002), and has only infrequently been applied to unfaulted clay-bearing rocks (Pevear, 1999; Grathoff et al., 2001). The outcomes from this study therefore highlight the potential to date gouge that does not only involve I–S to I transformation (see Vrolijk and van der Pluijm, 1999; van der Pluijm et al., 2001), but rather makes use of polytype transformation as well.

4. Results

4.1. Polytypism and I–S results

Relative proportions of illite polytype and discrete illite vs. I–S are plotted in Fig. 6. Discrete illite plus mixed-layer I–S are summed to 100%, and $2M_1$ illite plus $1M_d$ illite to 100%. The Mesozoic protolith is characterized by low concentrations of both discrete illite (15–55%) and $2M_1$ illite (5–37%). These samples are characterized by mixed-layer $1M_d$ I–S. The more-mature Paleozoic protolith is characterized by greater concentrations of both discrete illite (80–100%) and $2M_1$ illite (45–85%), the latter undifferentiated from $2M_1$ muscovite. The progression from mixed-layer $1M_d$ I–S to discrete $2M_1$ illite is in agreement with the expected progression from $2M_1$-poor, I–S-rich material to $2M_1$-rich, I–S-poor material with

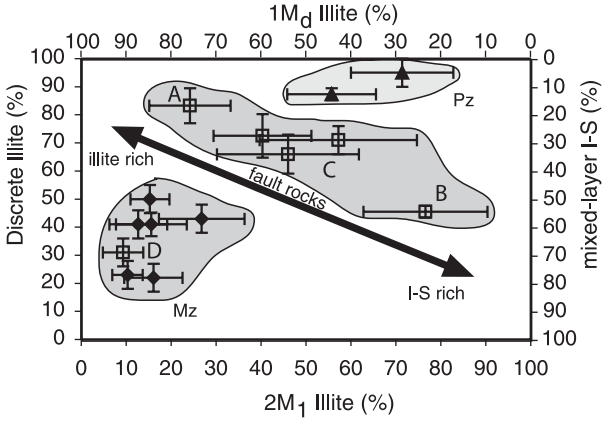

Fig. 6. Clay mineral assemblages from the study area based on XRD. The Mesozoic clay-bearing protolith (Mz) is characterized by low concentrations of both discrete illite and $2M_1$ illite. The more mature Paleozoic protolith (Pz) is characterized by greater concentrations of both discrete illite and undifferentiated $2M_1$ illite/muscovite. The most intensely deformed rocks (point A) are enriched in discrete illite, but contain very little $2M_1$ illite (labeled 'illite-rich'), while lesser-deformed rocks from the damage zone (points B and C) contain large amounts of $2M_1$ illite and little discrete illite, and therefore correspondingly greater amounts of I–S (labeled 'I–S-rich'). The single sample of fault rock that plots with the Mesozoic protolith (point D) is from the minor fault strand, and is likely a relatively unaltered piece of protolith that has been mechanically incorporated into the fault zone.

increasing metamorphic grade (Arkai et al., 1996; Merriman and Peacor, 1999). The gouge from the main strand (point A on Fig. 6) is composed of 24% $2M_1$ illite and 83% discrete illite (in other words it is composed largely of discrete $1M_d$ illite). A sample from the damage zone between the Cutler formation and the major gouge zone (point B on Fig. 6) is composed of 77% $2M_1$ illite and 46% discrete illite (this material is composed in part of mixed-layer $2M_1$ illite smectite). The rest of the samples from the damage zone (C on Fig. 6) plot on a line between the Paleozoic and Mesozoic protolith, as does one sample from the minor gouge zone. One sample from the minor gouge zone plots with the Mesozoic protolith (D on Fig. 6).

4.2. Clay fabrics

XTG analysis shows that clay fabrics in fault rocks from the Moab Fault are poorly developed, and, in fact, have been degraded by up to ~65% from the Cutler Group host rock (Fig. 7), although the difference is less pronounced compared with the Morrison Formation host rock. Back-scattered electron (BSE) SEM images show that large (up to ~100 μm) grains of muscovite (equivalent to $2M_1$ illite for the purposes of this study) and biotite generally form a well-defined fabric that is bedding-parallel in both Mesozoic and Paleozoic protoliths (Fig. 8A and B). In contrast, there is no clear foliation fabric in the damage zone (Fig. 8C), compatible with XTG measurements; however, there are a few poorly defined, discontinuous I–S shears in a matrix of cataclastically deformed protolith. Significantly, there is also no pronounced fabric apparent in the gouge (Fig. 8D). While foliation is visible on the BSE images, the orientation is variable. Reworked clasts of gouge are present, and the orientation of foliation in these clasts relative to the fault is random. Fabric intensities in Moab protolith and fault rocks are plotted relative to the values from other fault zones in Fig. 9. The significance of the low degree of preferred orientation is discussed below.

4.3. Gouge dating

The age analysis plot from the Moab Fault samples is depicted in Fig. 10, and data are listed in Table 2. The age of the neoformed $1M_d$ illite in the gouge is well defined at ~63±2 Ma (point A on Fig. 6), and the age of the neoformed illite–smectite in the I–S-rich region adjacent to the gouge (i.e. the damage zone) is similarly well constrained at ~60±2 Ma (point B on Fig. 6). As clay neomineralization in the gouge is characterized by $1M_d$ illite neoformation, the proportion of detrital and neoformed phases in the gouge are determined by measuring polytypes. As the neomineralization in the damage zone is characterized by I–S neoformation, the proportions of detrital and authigenic material in that area is quantified by determining the abundances of mixed-layer I–S and discrete illite. Beside Ar dating uncertainties, errors on these age determinations are largely dependent on the reliability of the illite compositional analysis. We conservatively assume an error of ±3% for compositional work based on an absolute precision of 2–5% reported for the polytype quantification method (Grathoff and Moore, 1996), which would result in an age error that is on the order of ±2 my. Thus, the age of both gouge and neighboring fractured host, obtained from age analyses of compositionally distinct samples, are statistically indistinguishable, giving an early Paleocene age for the formation of these fault rocks.

Table 2
Information for illite age analysis of a sample of gouge and a sample from the damage zone

Gouge (MB001-3)			
Size fraction	% Detrital ($2M_1$)	Total gas age (Ma)	$\exp(\lambda t)-1$
Coarse (0.5–<2 μm)	21.6	244.2	0.1449
Medium (0.05–<0.5 mm)	8.44	141.0	0.0813
Fine (<0.05 mm)	2.4	80.7	0.0457
Authigenic age (0% $2M_1$ illite) 62.7±2 Ma			
Detrital age (100% $2M_1$ illite) 786.8±24 Ma			
Damage zone (MB001-6)			
Size fraction	% Detrital (discrete illite)	Total gas age (Ma)	$\exp(\lambda t)-1$
Coarse (0.5–<2 μm)	36.9	213.7	0.1258
Medium (0.05–<0.5 mm)	19.04	122.5	0.0703
Fine (<0.05 mm)	4.22	86.0	0.0488
Authigenic age (0% discrete illite) 60.1±2 Ma			
Detrital age (100% discrete illite) 433.8±13 Ma			

5. Discussion

Many workers have attributed the existence of gouge to mostly mechanical processes. For example, gouge along the Moab Fault is referred to as 'shale smear' by Garden et al. (2001). Foxford et al. (1998) attributed the origin of clay gouge in this location to mechanical incorporation of pre-Wingate Formation shale units (such as the Triassic Chinle and Moenkopi Formations, the Permian Cutler Group, and the Pennsylvanian Honaker Trail Formation). A characteristic of all of these formations is that they contain abundant detrital mica (i.e. $2M_1$ muscovite/illite). Therefore, if the gouge is mechanically derived from these formations it should similarly contain abundant $2M_1$ illite, which is not observed. As shown in Fig. 6, the samples from the $2M_1$-rich Cutler group do not plot with the samples of gouge from the major strand of the fault or with samples from the intervening damage zone, indicating that fault-related clay mineral transformations have occurred. It is possible that the gouge is the result of mixing of Paleozoic protolith with the $2M_1$-poor Mesozoic shales. However, the clay mineral assemblages from fault rocks do not plot on a line connecting Paleozoic and Mesozoic protoliths, indicating that these mineral assemblages cannot be solely the result of

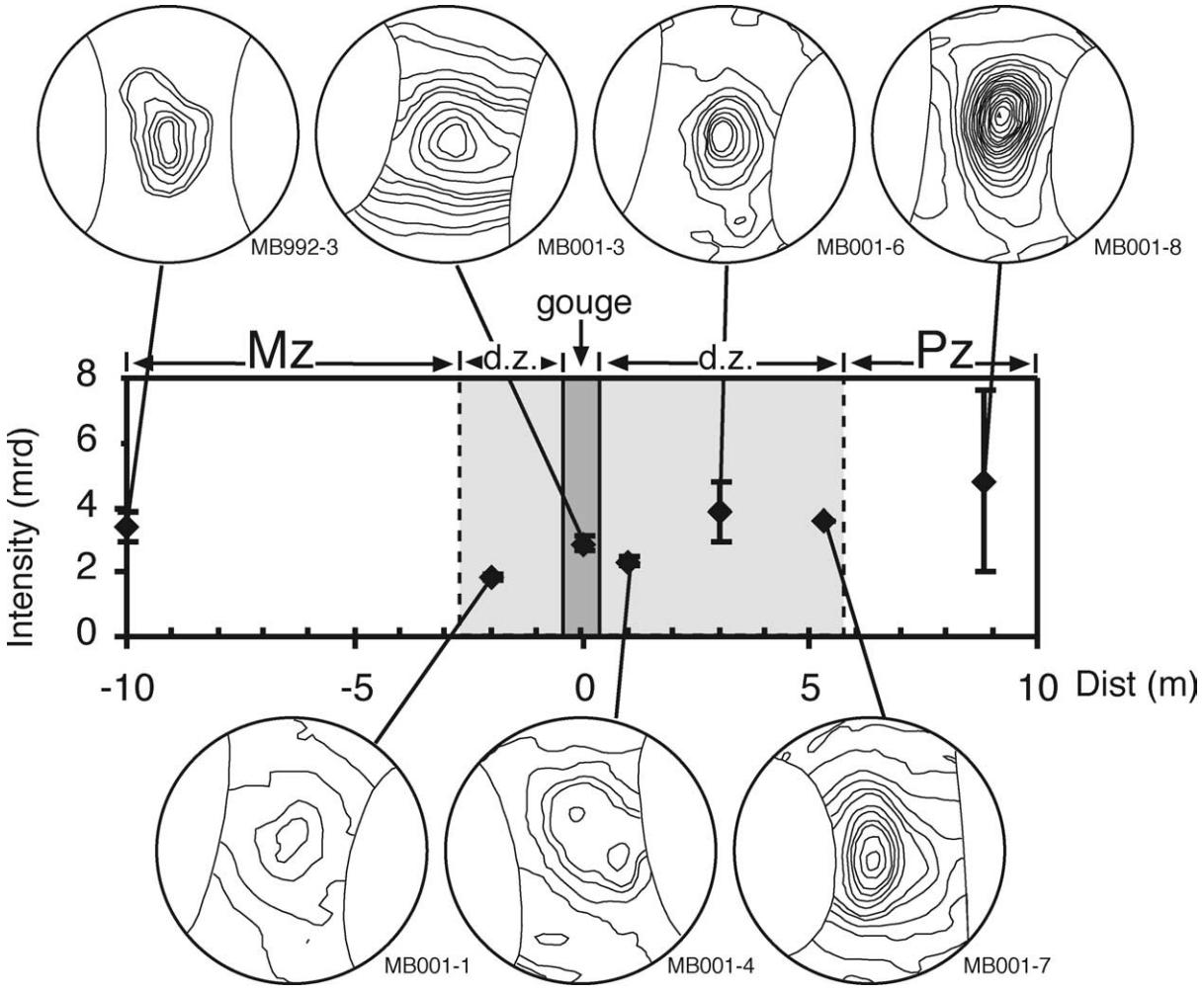

Fig. 7. Representative XTG pole figures and summary fabric intensities plotted on a schematic cross-section through the Moab Fault zone with Mesozoic protolith (hanging wall) on the left (labeled 'Mz') and Paleozoic protolith (footwall) on the right (labeled 'Pz'). The values from the fault core are denoted by a gray box labeled 'gouge', while the damage zone is denoted by a lighter gray box labeled 'd.z.'. The fabric intensities in fault rocks are low (~1.8–5 MRD compared with ~3–8 MRD in protolith).

mixing of Mesozoic and Paleozoic protoliths. Rather, our results indicate that fault-related changes in mineral species occurred. The most intensely deformed rocks (i.e. gouge from the major strand—point A on Fig. 6) are enriched in discrete $1M_d$ illite and contain very little $2M_1$ illite (a 'fingerprint' of the protoliths discussed above), whereas the lesser deformed samples from the damage zone between the major strand and the Cutler Formation (point B on Fig. 6) contain little discrete illite, and relatively little $1M_d$ illite (and therefore correspondingly greater amounts of I–S).

Foxford et al. (1998) attributed the gouge in the minor strand to clays mechanically derived from the Morrison Formation. Unlike gouge along the major strand, a sample from the minor strand plots with samples from that formation (point C on Fig. 6), which supports the idea that this gouge was mechanically derived. In addition, another sample from that minor strand (point D on Fig. 6) contains significant $2M_1$ illite, which is interpreted as a signature of the Triassic or Paleozoic protolith, as discussed above. It is therefore possible that this sample represents material mechanically derived from those formations. The two samples that plot near point B are from the damage zone/major fault core contact and possibly represent similar mechanically incorporated material.

The XTG fabric measurements eliminate fault rock anisotropy caused by clay as a mechanism that would allow fluids to be confined to the core of the Moab Fault (i.e. to be isolated from fluids in the damage zone or protolith). This eliminates a mechanism by which high pressure fluids could have been confined to the core of the Moab Fault (assuming such fluids existed). Interestingly, previous studies of quantitative fabric intensity in other fault zones have similarly revealed that clay fabrics in gouge are typically poorly developed (Vrolijk and van der Pluijm, 1999; Yan et al., 2001; Solum et al., 2003; Fig. 10). This lack of a well-developed fabric may be partially due to mechanical deformation and associated rotation of grains, but mostly by growth of clays without a significant preferred orientation.

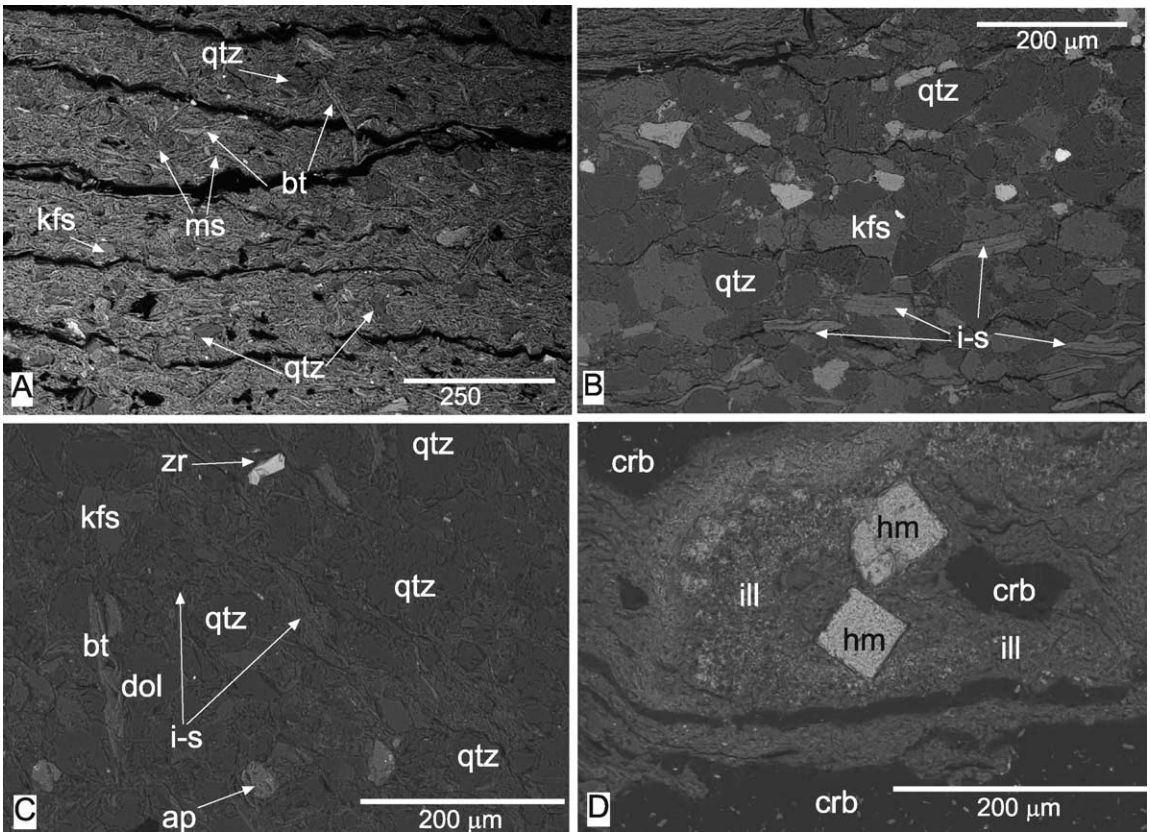

Fig. 8. BSE images of Paleozoic (A) and Mesozoic (B) protoliths. In both cases, large grains of detrital phyllosilicates are present, with muscovite (msv) and biotite (bt) in the Paleozoic protolith and illite/smectite (I–S) in the Mesozoic protolith that are approximately parallel to bedding (which is parallel to the bottom of the image). Muscovite can be distinguished from biotite in (A), as biotite is brighter than muscovite due to its greater mean atomic weight. Clasts of quartz (qtz) and K-feldspar (kfs) are also presented. The bright, high-Z clasts in the Mesozoic protolith are unidentified titanium, and/or uranium and vanadium-bearing minerals, as have been mined elsewhere in this unit, the Salt Wash member of the Morrison Formation. (C) BSE images from the damage zone between the fault core and the Paleozoic protolith. I–S, formed through the alteration of detrital micas, occurs in discontinuous poorly developed shears (labeled 'i–s'). zir, zircon; dlm, dolomite; apt, apatite; crb, carbon coating (due to sample preparation). (D) BSE images from the gouge zone. No large grains of phyllosilicates as seen in protolith and the damage zone are present. The gouge is a mixture of fine-grained illite (labeled 'ill') and other minerals too small to be easily distinguishable at the SEM scale, although based on XRD (e.g. Figs. 3 and 4), the gouge is composed of illite with minor amounts of kaolinite, hematite and quartz. The large square clasts labeled 'hm' are hematite, possibly pseudomorphs after pyrite. No well-developed, regular fabric is apparent in the gouge.

The widespread fault-related mineralization indicates a fluid-rich environment that promoted clay dissolution and new growth. Indeed, the occurrence of fluid flow along the Moab Fault is well established (e.g. Chan et al., 2000, 2001), although the pressure of those fluids is unknown. Garden et al. (2001) suggested that the Moab Fault acted as a seal for migrating hydrocarbons, allowing pressure to increase, although they state that the Moab Fault was not itself a conduit. We hypothesize that lateral fluid flux out of the illite-rich gouge zone (supralithostatic pressure or otherwise) was limited not by a clay fabric, but by neighboring illite–smectite-rich rocks that sealed the fault core. Morrow et al. (1984, fig. 3) found that a pure smectite sample and three natural I–S-bearing gouge samples have a water permeability of $\sim 3\text{–}6 \times 10^{-22}$ m^2 at a confining pressure of 200 MPa, while a pure illite sample has a permeability of $\sim 3 \times 10^{-21}$ m^2 under the same confining pressure. This is similar to the argon permeability of natural illite/chlorite/quartz gouge reported by Faulkner and Rutter (2001, fig. 1) of $\sim 10^{-19}$–10^{-21} m^2 at a confining pressure of 200 MPa and $\sim 10^{-18}$–10^{-20} m^2 at a confining pressure of 100 MPa. It is also possible that the permeability of the gouge is transiently increased by coseismic dilatancy. We argue that fluid in the gouge would be able to migrate freely along variable pathways, but are relatively confined to the gouge by the lower-permeability illite–smectite-rich damage zone. A schematic illustration of this proposed permeability structure of the fault zone is shown in Fig. 11. This hypothetical model is not intended to provide a quantitative model of the permeability structure of the Moab Fault zone, but offers a qualitative representation of the permeability structure of this fault. This model does not take into account fractures of deformation bands in sandstone (Davatzes et al., 2005), which also influence fault zone permeability. Similar to this scenario, others have proposed that mineral (silica or calcite) precipitation in fault zones forms seals that allow elevated fluid pressure to develop (Blanpied et al., 1992; Byerlee, 1993).

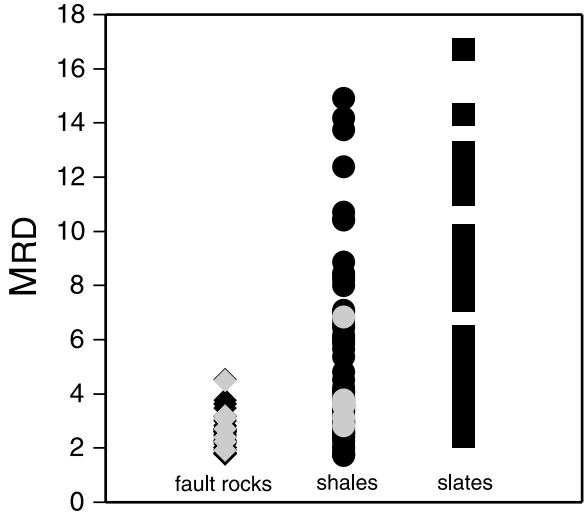

Fig. 9. Fabric intensities from a variety of geologic settings quantified using X-ray texture goniometry. Samples from Moab are shown as light gray symbols. Samples from other studies are shown in black (Solum et al., 2003).

Information on fault properties and mechanics from exhumed fault rocks requires that their characteristics are preserved from the time of faulting, which is determined by fabric dating. Stratigraphic relationships indicate that the Moab Fault was active intermittently from the late Paleozoic, through the Mesozoic and into the Tertiary. Whereas this part of the Colorado Plateau is seismically active, there is no evidence that the Moab Fault was active in the Quaternary (Olig et al., 1996; Wong et al., 1996). Our dating shows that Paleozoic and Mesozoic episodes of motion along the Moab Fault are not preserved, and that the last period of major activity along the fault occurred in the early Tertiary age. Pevear et al. (1997) reported ages of 50–60 Ma from K–Ar analysis of clay gouge along the northern section of the Moab Fault, whereas the Miocene age for mineral veins along the Moab Fault to the south (Chan et al., 2001) most likely represents mineralization associated with igneous activity in the nearby La Sal mountains, an interpretation suggested by these authors. The age of faulting reported in this study occurred just after the proposed time of maximum burial at ~60 Ma (Pevear et al., 1997), although the burial curves of Nuccio and Condon (1996) indicate that burial was not reached until ~40 Ma. Moreover, Garden et al. (2001) concluded that hydrocarbon migration in the Moab Anticline occurred at ~65 Ma, which is compatible with our age of 60–63 Ma, and the interpretation that associated changes in clay mineralogy in fault rocks are related to fluid flow. Beside the regional significance of the age, our dating confirms that the fabrics preserved in the exhumed fault zone rocks are ancient, permitting inferences about the behavior of the fault to be made from the observed mineral assemblages and fabrics. It should be noted that we are not attempting to directly relate fault-related clay mineralization to slip events; whether the mineralization occurred coseismically or postseismally cannot be determined from this study. Therefore, it is most accurate to say that the clay mineralization occurred during the period of time over which the fault was active.

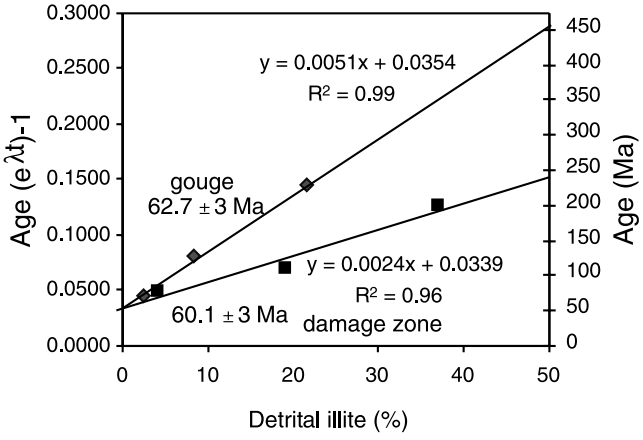

Fig. 10. Illite age analysis for the Moab Fault. The age and percent detrital illite of the coarse, medium and fine fractions are plotted, and an age that corresponds to 0% detrital/100% authigenic content is extrapolated, which corresponds to the age of neoformed illite, and therefore the age of the fault rocks. The age of neoformed $1M_d$ illite in the gouge (diamonds) is 62.7 ± 2 Ma, which is statistically indistinguishable from the age of neoformed I–S in the damage zone (squares) of 60.1 ± 2 Ma. This age reflects the most recent period of activity along this exposure of the Moab Fault, and indicates that the mineral assemblages and fabrics in the Moab Fault zone are not the result of recent alteration.

6. Conclusions

The results from this study of the Moab Fault demonstrate that faulting was responsible for >50% neocrystallized illite by dissolution and new growth in fault gouge and formation of I–S in the damage zone, requiring major fluid involvement. Thus, gouge is not merely the result of the mechanical incorporation of clays from the host rocks in the faulted stratigraphic sequence. Neocrystallization of clays permitted the application of two approaches to dating of the fault rocks, involving discrete illite/mixed-layer I–S dating for the damage zone and $2M_1/1M_d$ illite polytype dating for the fault core. Both approaches give overlapping results, showing that the latest period of faulting and fluid flow occurred at ~60–63 Ma, which agrees with earlier age analyses from locations elsewhere along the fault (Pevear et al., 1997) and coincides with the age of hydrocarbon migration in the Moab Anticline (Garden et al., 2001). The ages also indicate (1) that older fault-related mineral assemblages are reworked by younger events in the earliest Tertiary, and (2) that the present mineral assemblages and fabrics are ancient, and not the result of recent hydrothermal or diagenetic alteration. Regardless of the geological significance of these ages, this paper highlights the steps that should be taken to extract reliable dates from illite-bearing fault rocks.

The degree of phyllosilicate preferred orientation in

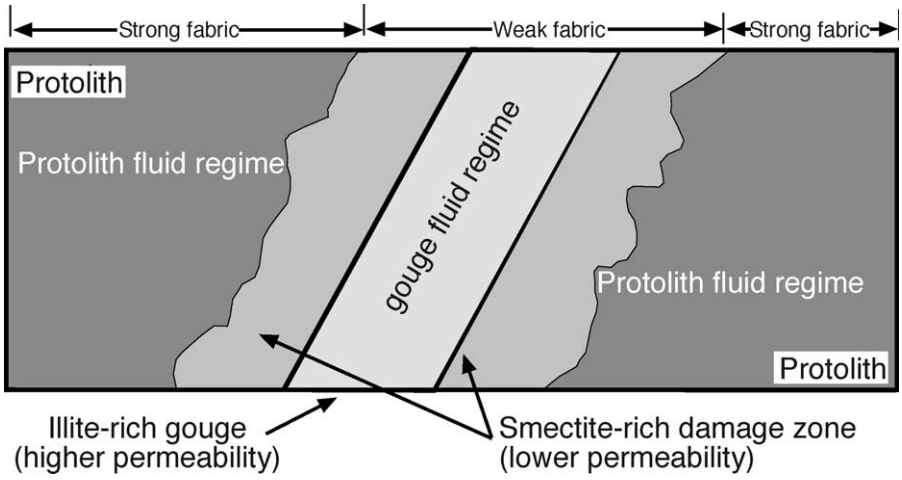

Fig. 11. Schematic illustration of the permeability structure of the fault zone and the influence of clay mineral assemblages and fabrics on fluid flow. We hypothesize that fluids were likely focused in the gouge zone, the region where most of the displacement was accommodated, by adjacent I–S-rich rocks. As discussed in the text, I–S has a lower permeability than discrete illite, and so while fluids would be able to migrate freely throughout the gouge, they would be confined to that zone.

these fault rocks decreases significantly from that in undeformed protolith. A potential mineralogical permeability contrast between I–S-bearing rocks in the damage zone and more illitic rocks in the gouge provides a mechanism by which fluids could be isolated in the fault core from fluids in the protolith.

Acknowledgements

This study was funded through NSF grants EAR-9980459 and EAR-0230055 and grants from the Scott M. Turner Fund at the University of Michigan. TEM and SEM work was completed at the University of Michigan Electron Microbeam Analysis Laboratory and Ar dating at the University of Michigan Radiogenic Isotope Geochemistry Laboratory. We thank Chris Hall for his assistance with Ar dating. We thank Laurence Warr for assistance with electron microscopy and discussion, Tracy Kolb for her assistance with sample preparation, and Kevin Thomas for assistance with collection of samples in the field. Peter Vrolijk and David Pevear provided early guidance with field sampling and clay analysis. Reviews by Jonathan Caine and Martha Gerdes clarified our presentation and improved an earlier version of the manuscript. Thoughtful reviews by Nick Hayman and Darrel Cowan of the final manuscript are appreciated.

References

Arkai, P., Merriman, R.J., Roberts, B., Peacor, D.R., Toth, M., 1996. Crystallinity, crystallite size and lattice strain of illite-muscovite and chlorite: comparison of XRD and TEM data for diagenetic to epizonal pelites. European Journal of Mineralogy 8, 1119–1137.

Blanpied, M.L., Lockner, D.A., Byerlee, J.D., 1992. An earthquake mechanism based on rapid sealing of faults. Nature 358, 574–576.

Byerlee, J.D., 1993. Model for episodic flow of high-pressure water in fault zones before earthquakes. Geology 21, 303–306.

Caine, J.S., Evans, J.P., Forster, C.B., 1996. Fault zone architecture and permeability structure. Geology 24, 1025–1028.

Chan, M.A., Parry, W.T., Bowman, J.R., 2000. Diagenetic hematite and manganese oxides and fault-related fluid flow in Jurassic sandstones, southeastern Utah. American Association of Petroleum Geologists Bulletin 84, 1281–1310.

Chan, M.A., Parry, W.T., Petersen, E.U., Hall, C.M., 2001. $^{40}Ar/^{39}Ar$ age and chemistry of manganese mineralization in the Moab and Lisbon fault systems, southeastern Utah. Geology 29, 331–334.

Davatzes, N.C., Aydin, A., 2005. Distribution and nature of fault architecture in a layered sandstone and shale sequence: an example from the Moab fault, Utah. In: Sorkhabi, R., Tsuji, Y. (Eds.), Faults, Fluid Flow, and Petroleum Traps. American Association of Petroleum Geologists Memoir, 85, pp. 153–180.

Davatzes, N.C., Eichhubl, P., Aydin, A., 2005. Structural evolution of fault zones in sandstone by multiple deformation mechanisms: Moab fault, southeast Utah. Geological Society of America Bulletin 117, 135–148.

Doelling, H.H., 1988. Geology of Salt Valley Anticline and Arches National Park, Grand County, Utah. In: Doelling, H.H., Oviatt, C.G., Huntoon, P.W. (Eds.), Salt Deformation in the Paradox Region, Utah Utah Geological and Mineral Survey Bulletin, vol. 122, pp. 1–60.

Doelling, H.H., 2001. Geologic map of the Moab and Eastern Part of the San Rafael Desert $30' \times 60'$ quadrangles, Grand and Emery counties, Utah and Mesa county, Colorado. Geologic map 180: Utah Geological Survey Geologic Map 180, scale 1:100,000.

Dong, H., Hall, C.M., Peacor, D.R., Halliday, A.N., 1995. Mechanisms of argon retention in clays revealed by laser ^{40}Ar–^{39}Ar dating. Nature 267, 355–359.

Evans, J.P., Forster, C.B., Goddard, J.V., 1997. Permeability of fault-related rocks, and implications for hydraulic structure of fault zones. Journal of Structural Geology 19, 1393–1404.

Faulkner, D.R., Rutter, E.H., 2001. Can the maintenance of overpressured fluids in large strike-slip fault zones explain their apparent weakness? Geology 29, 503–506.

Foxford, K.A., Garden, I.R., Guscott, S.C., Burley, S.D., Lewis, J.J.M., Walsh, J.J., Watterson, J., 1996. The field geology of the Moab Fault.

In: Huffman Jr., A.C., Lund, W.R., Goodwin, L.H. (Eds.), Geology and Resources of the Paradox Basin Utah Geological Association Guidebook 25. Salt Lake City, pp. 265–283.

Foxford, K.A., Walsh, J.J., Watterson, J., Garden, I.R., Guscott, S.C., Burley, S.D., 1998. Structure and content of the Moab fault zone, Utah, USA, and its implications for fault seal prediction. In: Jones, G., Fisher, Q.J., Knipe, R.J. (Eds.), Faulting, Fault Sealing and Fluid Flow in Hydrocarbon Reservoirs Geological Society of Special Publication, vol. 147, pp. 87–103.

Garden, I.R., Guscott, S.C., Burley, S.D., Foxford, K.A., Walsh, J.J., Marshall, J., 2001. An exhumed palaeo-hydrocarbon migration fairway in a faulted carrier system, Entrada Sandstone of SE Utah, USA. Geofluids 1, 195–213.

Grathoff, G.H., Moore, D.M., 1996. Illite polytype quantification using WILDFIRE—calculated patterns. Clays and Clay Minerals 44, 835–842.

Grathoff, G.H., Moore, D.M., Lay, R.L., Wemmer, K., 1998. Illite polytype quantification and K/Ar dating of Paleozoic shales: a technique to quantify diagenetic and detrital illite. In: Schieber, J., Zimmerle, W., Sethi, P. (Eds.), Shales and Mudstones II. E. Schweizerbart'sche Verlagsbuchhandlung (Nägele u. Obermiller), Stuttgart, pp. 161–175.

Grathoff, G.H., Moore, D.M., Hay, R.L., Wemmer, K., 2001. Origin of illite in the lower Paleozoic of the Illinois basin: evidence for brine migrations. Geological Society of America Bulletin 113, 1092–1104.

Hayman, N.W., Housen, B.A., Cladouhos, T.T., Livi, K., 2004. Magnetic and clast fabrics as measurements of grain-scale processes with the Death Valley shallow crustal detachment faults. Journal of Geophysical Research 109, B05409. doi:10.1029/2003JB002902.

Hower, J., Hurley, P.M., Pinson, W.H., Fairbairn, H.W., 1963. The dependence of K–Ar age on the mineralogy of various particle size ranges in a shale. Geochimica et Cosmochimica Acta 27, 405–410.

Hubbert, M.K., Rubey, W.W., 1959. Role of fluid pressure in mechanics of overthrust faulting. Geological Society of America Bulletin 70, 15–166.

Huntoon, P.W., 1988. Late Cenozoic gravity tectonic deformation related to the Paradox salts in the Canyonlands area of Utah. In: Doelling, H.H., Oviatt, C.G., Huntoon, P.W. (Eds.), Salt Deformation in the Paradox region, Utah Utah Geological and Mineral Survey Bulletin, vol. 122, pp. 79–93.

Jones, R.M., Hillis, R.R., 2003. An integrated, quantitative approach to assessing fault-seal risk. American Association of Petroleum Geologists Bulletin 87, 507–524.

Kanamori, H., Anderson, D.L., 1975. Theoretical basis of some empirical relations in seismology. Bulletin of the Seismological Society of America 65, 1073–1095.

Lachenbruch, A.H., Sass, J.H., 1980. Heat flow and energetics of the San Andreas fault zone. Journal of Geophysical Research 85, 6185–6222.

Lyons, J.B., Snellenberg, J., 1971. Dating faults. Geological Society of America Bulletin 82, 1749–1751.

Merriman, R.J., Peacor, D.R., 1999. Very low-grade metapelites: mineralogy, microfabrics and measuring reaction progress. In: Frey, M., Robinson, D. (Eds.), Low-Grade Metamorphism. Blackwell Science, London, pp. 10–60.

Moore, D.M., Reynolds Jr., R.C., 1997. X-ray Diffraction and the Identification and Analysis of Clay Minerals. Oxford University Press, Oxford.

Morrow, C.A., Shi, L.Q., Byerlee, J.D., 1984. Permeability of fault gouge under confining pressure and shear stress. Journal of Geophysical Research 89, 3193–3200.

Mount, V., Suppe, J., 1987. State of stress near the San Andreas fault: implications for wrench tectonics. Geology 15, 1143–1146.

Nuccio, V.F., Condon, S.M., 1996. Burial and thermal history of the Paradox Basin, Utah and Colorado, and petroleum potential of the Middle Pennsylvanian Paradox Basin, US Geological Survey Bulletin, 2000-O 1996. 41pp.

Olig, S.S., Fenton, C.H., McCleary, J., Wong, I.G., 1996. The earthquake potential of the Moab Fault and its relation to salt tectonics in the Paradox Basin, Utah. In: Huffman Jr., A.C., Lund, W.R., Goodwin, L.H. (Eds.), Geology and Resources of the Paradox Basin Utah Geological Association Guidebook 25, Salt Lake City, pp. 251–264.

Oviatt, C.G., 1988. Evidence for Quaternary deformation in the Salt Valley Anticline, southeastern Utah. In: Doelling, H.H., Oviatt, C.G., Huntoon, P.W. (Eds.), Salt Deformation in the Paradox region, Utah Utah Geological and Mineral Survey Bulletin, vol. 122, pp. 61–78.

Parry, W.T., Bunds, M.P., Bruhn, R.L., Hall, C.M., Murphy, J.M., 2001. Mineralogy, $^{40}Ar/^{39}Ar$ dating and apatite fission track dating of rocks along the Castle Mountain fault, Alaska. Tectonophysics 337, 149–172.

Peacor, D.R., Bauluz, B., Dong, H., Tillick, D., Yan, Y., 2002. TEM and AEM evidence for high Mg contents of 1M illite. Absence of 1M polytypism in normal prograde diagenetic sequences. Clays & Clay Minerals 50, 757–765.

Pevear, D.R., 1999. Illite and hydrocarbon exploration. Proceedings of the National Academy of Sciences 96, 3440–3446.

Pevear, D.R., Vrolijk, P.J., Longstaffe, F.J., 1997. Timing of Moab Fault displacement and fluid movement intergrated with burial history using radiogenic and stable isotopes. In: Hendry, J., Carey, P., Parnell, J., Ruffell, A., Worden, R. (Eds.), Geofluids II '97: Contributions to the Second International Conference on Fluid Evolution, Migration and Interaction in Sedimentary Basins and Orogenic Belts, Belfast, pp. 42–45.

Reynolds Jr., R.C., Reynolds III., R.C., 1996. NEWMOD-for-Windows. The Calculation of One-Dimensional X-ray Diffraction Patterns of Mixed-layered Clay Minerals, Hanover, New Hampshire 1996.

Rice, J.R., 1992. Fault stress states, pore pressure distributions, and the weakness of the San Andreas Fault. In: Evans, B., Wong, T.-f. (Eds.), Fault Mechanics and Transport Properties of Rocks; A Festschrift in Honor of W.F. Brace. Academic Press, San Diego, pp. 475–503.

Scruggs, V.J., Tullis, T.E., 1998. Correlation between velocity dependence of friction and strain localization in large displacement experiments on feldspar, muscovite and biotite gouge. Tectonophysics 295, 15–40.

Sibson, R.H., 1990. Conditions for fault-valve behaviour. In: Knipe, R.J., Rutter, E.H. (Eds.), Deformation Mechanisms, Rheology and Tectonics Geological Society Special Publication, vol. 54, pp. 15–28.

Sibson, R.H., 2003. Brittle-failure controls on maximum sustainable overpressure in different tectonic regimes. AAPG Bulletin 87, 901–908.

Solum, J.G., 2005. Clay neomineralization in fault zones: extracting information of fault properties and timing. PhD thesis, University of Michigan.

Solum, J.G., van der Pluijm, B.A., Peacor, D.R., Warr, L.N., 2003. Influence of phyllosilicate mineral assemblages, fabrics, and fluids on the behavior of the Punchbowl fault, southern California. Journal of Geophysical Research 108, 2233. doi:10.1029/2002JB001858.

van der Pluijm, B.A., Ho, N.-C., Peacor, D.R., 1994. High-resolution X-ray texture goniometry. Journal of Structural Geology 16, 1029–1032.

van der Pluijm, B.A., Hall, C.M., Vrolijk, P.J., Pevear, D.R., Covey, M.C., 2001. The dating of shallow faults in the Earth's crust. Nature 412, 172–175.

Velde, B., Hower, J., 1963. Petrological significance of illite polymorphism in Paleozoic sedimentary rocks. American Mineralogist 48, 1239–1254.

Vrolijk, P., van der Pluijm, B.A., 1999. Clay gouge. Journal of Structural Geology 21, 1039–1048.

Wang, C.-Y., 1984. On the constitution of the San Andreas fault zone in central California. Journal of Geophysical Research 89, 5858–5866.

Wenk, H.-R., 1985. Preferred Orientation in Deformed Metals and Rocks: An Introduction to Modern Texture Analysis. Academic Press, Orlando.

Wong, I.G., Olig, S.S., Bott, J.D.J., 1996. Earthquake potential and seismic hazards in the Paradox Basin, southeastern Utah. In: Huffman Jr., A.C., Lund, W.R., Goodwin, L.H. (Eds.), Geology and Resources of the Paradox Basin Utah Geological Association Guidebook 25: Salt Lake City, pp. 241–250.

Yan, Y., van der Pluijm, B.A., Peacor, D.R., 2001. Deformation microfabrics of clay gouge, Lewis Thrust, Canada: a case for fault weakening from clay transformation. In: Holdsworth, R.E.,

Strachan, R.A., Magloughlin, J.F., Knipe, R.J. (Eds.), The Nature and Tectonic Significance of Fault Zone Weakening Geological Society Special Publication, vol. 186, pp. 103–112.

Yielding, G., Freeman, B., Needham, D.T., 1997. Quantitative fault seal prediction. American Association of Petroleum Geologists Bulletin 81, 897–917.

Ylagan, R.F., Kim, C.S., Pevear, D.R., Vrolijk, P.J., 2002. Illite polytype quantification for accurate K–Ar age determination. American Mineralogist 87, 1536–1545.

Zhang, S., Cox, S.F., 2000. Enhancement of fluid permeability during shear deformation of a synthetic mud. Journal of Structural Geology 22, 1385–1393.

Zhang, S., Tullis, T.E., Scruggs, V.J., 1999. Permeability anisotropy and pressure dependency of permeability in experimentally sheared gouge materials. Journal of Structural Geology 21, 795–806.

Zoback, M.D., 2000. Strength of the San Andreas Fault. Nature 405, 31–32.

Zoller, M., Brockamp, O., 1997. 1M and $2M_1$ illites: different minerals and not polytypes. European Journal of Mineralogy 9, 821–827.

Zwingmann, H., Offler, R., Wilson, T., Cox, S.F., 2004. K–Ar dating of fault gouge in the northern Sydney Basin, NSW, Australia—implications for the breakup of Gondwana. Journal of Structural Geology 26, 2285–2295.